

Use of optoelectronic tweezers in manufacturing—accurate solder bead positioning

Shuailong Zhang, Yongpeng Liu, Joan Juvert, Pengfei Tian, Jean-Claude Navarro, Jonathan M. Cooper, and Steven L. Neale

Citation: *Appl. Phys. Lett.* **109**, 221110 (2016); doi: 10.1063/1.4971348

View online: <http://dx.doi.org/10.1063/1.4971348>

View Table of Contents: <http://aip.scitation.org/toc/apl/109/22>

Published by the [American Institute of Physics](#)

Use of optoelectronic tweezers in manufacturing—accurate solder bead positioning

Shuailong Zhang,^{1,a)} Yongpeng Liu,¹ Joan Juvert,^{1,b)} Pengfei Tian,² Jean-Claude Navarro,³ Jonathan M. Cooper,¹ and Steven L. Neale¹

¹School of Engineering, University of Glasgow, Glasgow G12 8LT, United Kingdom

²Institute for Electric Light Sources, Fudan University, Shanghai 200433, China

³IPS, 24A, rue de la Résistance, BP 438, 74108 ANNEMASSE Cedex, France

(Received 27 October 2016; accepted 19 November 2016; published online 2 December 2016)

In this work, we analyze the use of optoelectronic tweezers (OETs) to manipulate 45 μm diameter $\text{Sn}_{62}\text{Pb}_{36}\text{Ag}_2$ solder beads with light-induced dielectrophoresis force and we demonstrate high positioning accuracy. It was found that the positional deviation of the solder beads increases with the increase of the trap size. To clarify the underlying mechanism, simulations based on the integration of the Maxwell stress tensor were used to study the force profiles of OET traps with different sizes. It was found that the solder beads felt a 0.1 nN static friction or stiction force due to electrical forces pulling them towards the surface and that this force is not dependent on the size of the trap. The stiction limits the positioning accuracy; however, we show that by choosing a trap that is just larger than the solder bead sub-micron positional accuracy can be achieved. © 2016 Author(s). All article content, except where otherwise noted, is licensed under a Creative Commons Attribution (CC BY) license (<http://creativecommons.org/licenses/by/4.0/>). [<http://dx.doi.org/10.1063/1.4971348>]

Optoelectronic tweezers (OETs) have been demonstrated as a useful opto-electro-fluidic technology utilizing light-induced dielectrophoresis (DEP) for micromanipulation applications.¹ Apart from being useful for biological applications such as cell sorting and cell patterning,^{1–3} the capability of moving small objects accurately and assembling them into arbitrary 2D patterns also makes OETs an attractive approach for microassembly applications. Previous OET studies have demonstrated the successful assembly of various nanoscale components, such as semiconductor nanowires,⁴ metallic nanowires,^{4,5} and metallic spherical nanocrystals.⁶ However, there is a growing interest in using OETs to manipulate and assemble large photonic and electronic components with scales of one or several hundreds of microns, such as standard semiconductor microlasers⁷ and surface-mount-technology (SMT) capacitors.⁸ To build up a photonic or an electronic device containing such large components, it is desirable to use metallic objects with scales of several tens of microns to form a conductive link as this cuts down the number of interfaces between conductive components reducing the chances of a poor connection and associated high resistance. In this work, we analyze the use of OET traps with different sizes to manipulate 45 μm diameter $\text{Sn}_{62}\text{Pb}_{36}\text{Ag}_2$ solder beads with strong DEP force and high positioning accuracy. It is found that there is a dependence of positioning accuracy on the size of the trap, which is due to the competition between the stiction force and the DEP force of a trap with a specific force profile. The experimental work is also supported by simulations in COMSOL_Multiphysics 5.0 (COMSOL Inc., USA).

Figure 1(a) shows the cross-sectional schematic of the OET device used in this work consisting of two electrodes,

both of them are glass slide coated with 600 nm thick indium tin oxide (ITO) (Diamond Coatings, UK). The bottom electrode is also coated with an additional 1 μm thick hydrogenated amorphous silicon (a-Si:H) photoconductive layer by plasma-enhanced chemical vapour deposition. The two electrodes are vertically mounted together with a spacer to create a 150 μm thick chamber between the electrodes. The experimental setup is the same as previously reported work:⁷ a light pattern from a digital micro-mirror device (DMD) projector (Dell 1510X) is introduced into a microscope (Olympus BX51, with motorised Prior Scan111 stage) and imaged onto the OET device, which is driven by the amplified signal from the function generator (TG5011 LX1 with amplifier Thurlby

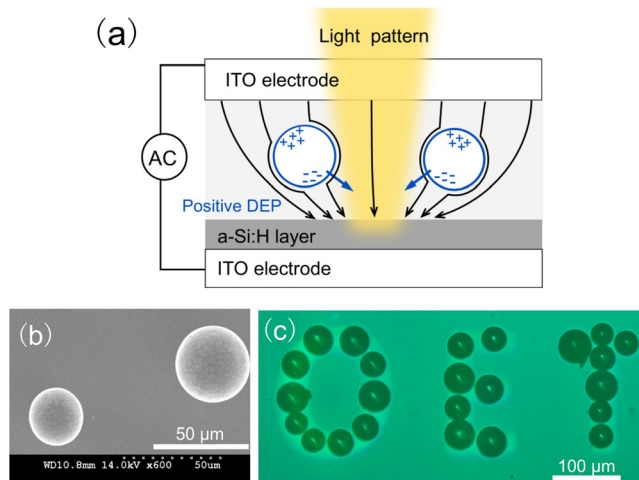


FIG. 1. (a) Schematic diagram of the OET device used in this work. The black arrows show the non-uniform electric field resulting from the resistivity change caused by the illumination of the a-Si:H layer. The solder beads, represented by the blue circles, are attracted to the illuminated area under positive DEP force; (b) SEM image of the solder beads; and (c) “OET” pattern formed by solder beads being attracted to the illuminated region via positive DEP force.

^{a)}Electronic mail: petershuailong@gmail.com

^{b)}Present address: Photonics Research Group, Center for Nano- and Biophotonics (NB-Photonics), INTEC-department, Ghent University-IMEC, Technologiepark-Zwijnaarde 15 iGent, 9052 Gent, Belgium.

Thandor Instrument WA31). Figure 1(b) shows the scanning electron microscopy (SEM) image of the $\text{Sn}_{62}\text{Pb}_{36}\text{Ag}_2$ solder beads (Industrie des Poudres Sphériques, France) used in this work. To perform the experiment, the solder beads were put into a solution containing deionized water and a volume ratio of 0.05% non-ionic surfactant “TWEEN 20” (SIGMA P9416). Then, the solution containing solder beads was pipetted into the chamber of the OET device. To functionalize the OET device, a 15 kHz 25 V peak-to-peak AC voltage was applied, similar to the bias conditions used to manipulate other metallic particles in the OET device.^{5,8} On applying the AC, the solder beads were attracted to the illumination region due to the positive DEP force, as shown in Figure 1(c). As provided by the company, the beads have a wide size range from 20 μm to 110 μm . However, beads with sizes of 45 μm ($\pm 3 \mu\text{m}$) were selected for measuring the trap profile and studying positional accuracy.

Based on Stokes law, the viscous drag force of a solder bead can be calculated, which is equal to the DEP force in this viscously damped environment. To study the trap profile, the velocity of the light pattern trapping a solder bead was gradually increased until the bead fell out of the trap. Figures 2(a)–2(d) show the microscopy images of a solder bead trapped by 60 μm diameter and 140 μm diameter

circular light patterns at different velocities. As shown, the centre-to-centre distance (“D” in Figure 2(a)) between the bead and the light pattern increases as the velocity increases. By measuring the center-to-center distance at varying velocities, a trap profile can be plotted, which shows the DEP force experienced by a bead at different positions within the trap. It is worth mentioning that the solder beads have a density of 8 g/cm³, and the DEP force also pulls them down to the bottom of the chamber. Therefore, a reasonable assumption was made that the microspheres sit in proximity of the a-Si:H surface. Therefore, Faxen’s correction based on the radius of the microsphere (22.5 μm) was used to adjust the calculated DEP force.⁹ Figure 2(e) shows the measured trap profiles (data points) of a solder bead in circular light patterns with 60 μm , 100 μm , 140 μm , and 180 μm diameters. The error bar comes from the uncertainty in measuring the center-to-center distance between the bead and trap. As shown, the solder bead can be moved at a max velocity of 2500 $\mu\text{m/s}$ for all the traps, corresponding to a DEP force of 2.9 nN. This result matches up with the previously reported results of moving silver-coated Polymethyl methacrylate (PMMA) beads in an OET system: the large metallic beads can experience a very high DEP force in the regime of several nano newtons (10^{−9} N), which is due to the large size of the bead and the influence of its metal surface on the surrounding electric field.⁸ The simulated trap profiles (solid lines) are also presented in Figure 2(e), which will be discussed later.

The strong DEP force is very useful for positioning solder beads as it means we can quickly move them into position. However, before assembling or patterning these beads for applications such as circuit construction, it is important to study the achievable positioning accuracy of solder beads and the factors influencing the accuracy. Therefore, we confine a solder bead in an OET trap and find the positions of the trap center and bead center by superimposing a best-fit circular ring to the boundaries of the bead and trap using the microscope’s image analysing software (Cell Sense Standard, Olympus). Then, the trap with the bead was moved to a new position a few hundred microns away, and the positions of the bead center and trap center were measured again. We repeat this process of random movement and measurement of the positions several times for circular traps with different sizes and calculate the distance between the bead center and trap center in its X and Y components, which are denoted as X offset and Y offset. If the bead follows the trap perfectly as it moves, these offsets would be zero. Figures 3(a)–3(f) show the X offset and Y offset of the centre of a solder bead with respect to the centre of a trap for traps with different sizes. As shown, both X and Y offsets of the solder bead generally increase with the increase of trap size, indicating that the solder bead is less well confined to the central region. The confining capability of the central region of a trap is related to the positioning accuracy of the solder bead, as it determines the deviation between the bead and trap when it is moved to a random position. In this work, we defined the positioning accuracy of the solder bead based on positioning deviation between the bead and trap, which is numerically calculated from the average travelling difference between the bead and the trap when the trap is moved between different random positions. This was calculated as

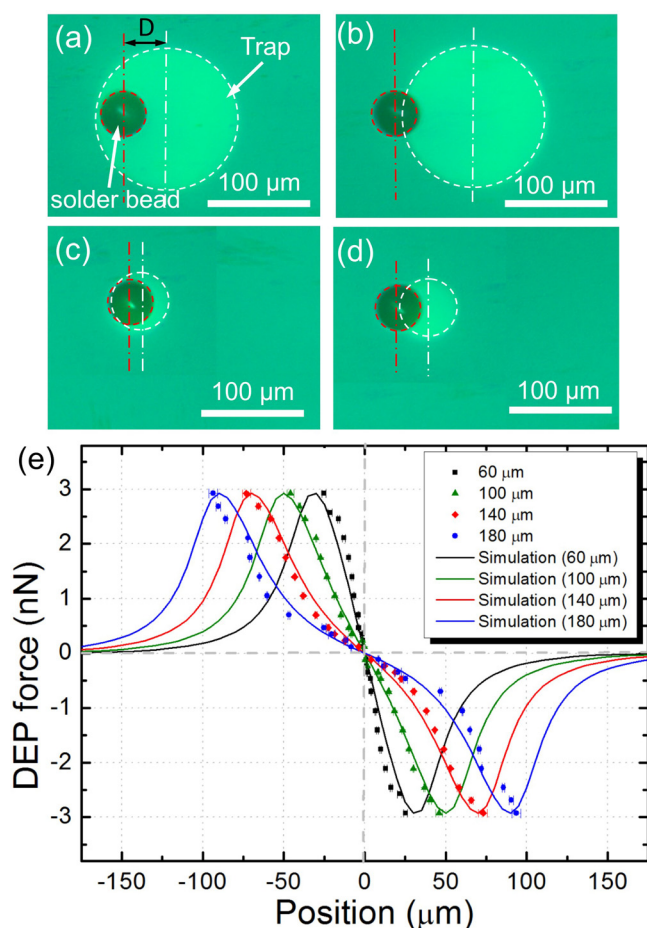


FIG. 2. (a) Microscopy images of a solder bead trapped by 140 μm diameter circular light pattern at (a) 900 $\mu\text{m/s}$ and (b) 2500 $\mu\text{m/s}$; microscopy images of a solder bead trapped by 60 μm diameter circular light pattern at (c) 1200 $\mu\text{m/s}$ and (d) 2500 $\mu\text{m/s}$; and (e) measured trap profiles (data points) and simulated trap profiles (solid lines) of a solder bead created by 60 μm , 100 μm , 140 μm , and 180 μm diameter light patterns.

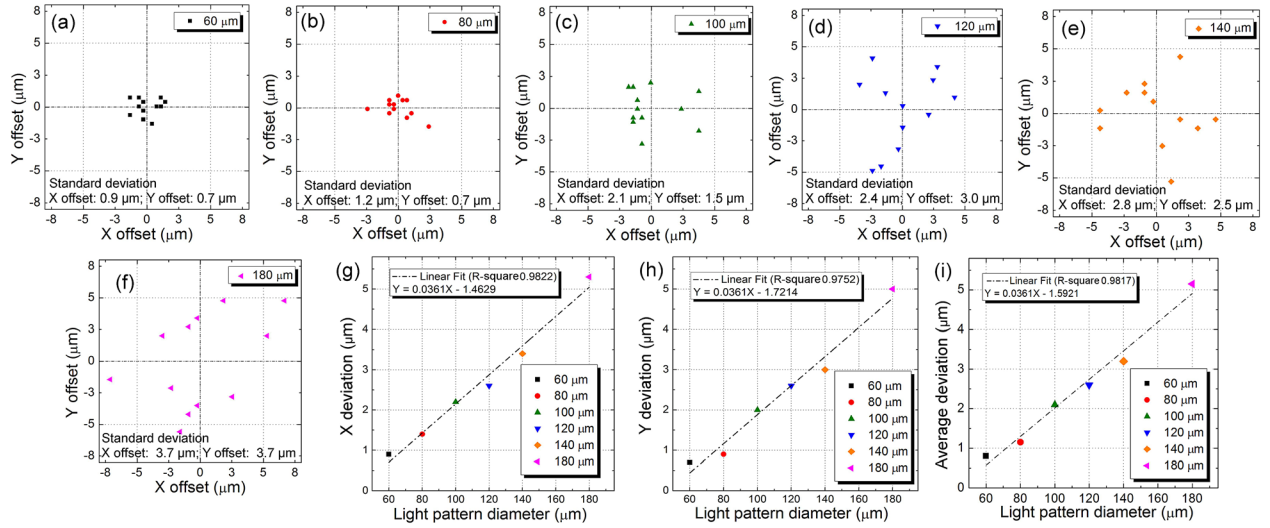


FIG. 3. X offset and Y offset of the center of a solder bead with respect to the center of the circular trap with a diameter of (a) 60 μm , (b) 80 μm , (c) 100 μm , (d) 120 μm , (e) 140 μm , and (f) 180 μm ; (g) positioning accuracy of the solder bead in the X direction for traps with different sizes; (h) positioning accuracy of the solder bead in the Y direction for traps with different sizes; and (i) average positioning accuracy of the solder bead for traps with different sizes.

$$X_{\text{deviation}} = \frac{\sum_{i=0}^N |X_{T(i+1)} - X_{T(i)}| - |X_{B(i+1)} - X_{B(i)}|}{N}, \quad (1)$$

$$Y_{\text{deviation}} = \frac{\sum_{i=0}^N |Y_{T(i+1)} - Y_{T(i)}| - |Y_{B(i+1)} - Y_{B(i)}|}{N}, \quad (2)$$

$$\text{Aver}_{\text{deviation}} = \frac{X_{\text{deviation}} + Y_{\text{deviation}}}{2}. \quad (3)$$

For Equation (1), $X_{\text{deviation}}$ represents the positioning deviation of the solder bead in the X direction, N is the total times of random movement, $X_{T(i)}$ is the center position of the trap in the X direction in position Number i , and $X_{B(i)}$ is the center position of the solder bead in the X direction in position Number i . Equation (2) describes a similar situation for the Y direction. In Equation (3), $\text{Aver}_{\text{deviation}}$ represents the average positioning deviation. Based on these equations, we can calculate the positioning deviation of a solder bead in X and Y directions and the average position deviation when the bead is positioned by traps with different sizes, as shown in Figures 3(g)–3(i). As shown, the positioning deviation of the solder bead increases linearly with the increase of the trap size, indicating the reduced capability of a larger trap to position the bead accurately. Interestingly, very similar linear relationships can be achieved for the positioning deviation in X and Y directions and also for the average positioning deviation. These results also show that the smallest trap we used, 60 μm diameter, produced a sub-micron positioning accuracy. We propose that the positioning accuracy is well represented by the boundary of a circular region where within the region the stiction force keeping the bead motionless dominates over the DEP force pushing the bead toward the trap centre. It is also expected that the position deviation of the bead in a trap should be similar in any direction under the co-effect of the stiction force and DEP force.

To further analyze the stiction force and the positioning accuracy of the solder bead, the OET trap profile was

simulated in COMSOL_Multiphysics 5.0 based on a previously reported 2D model.^{8,9} Due to the large size of the solder bead and the influence of its metallic surface on the electric field, the electrical potential (see Figure 4(a)) and electric field vary significantly across the solder bead, which makes the usual assumption that the field varies little over the particle inappropriate.⁸ To solve this problem, a calculation method based on the integration of the Maxwell stress tensor over the surface of the bead was used, which takes the variation of electric field into account and has been proven to be successful for calculating the DEP force of large

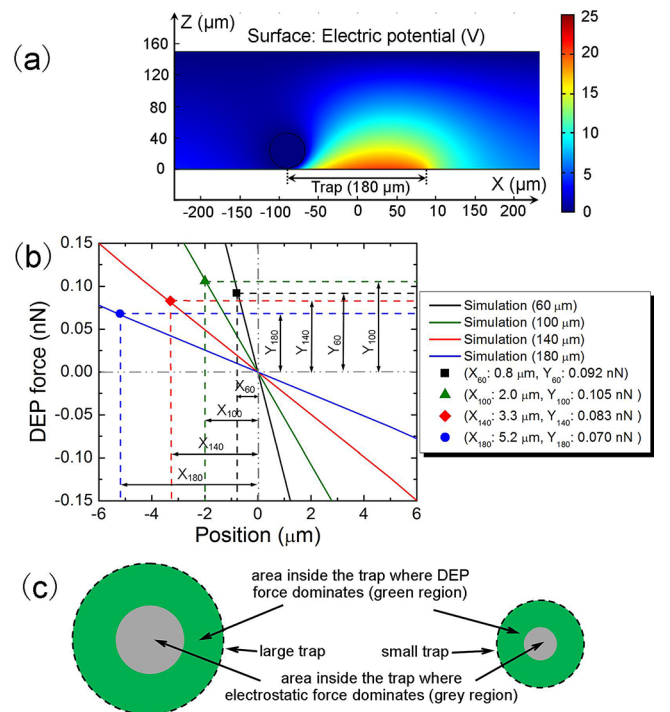


FIG. 4. (a) Simulated electrical potential distribution of the OET device with a solder bead at the left edge of the trap; (b) simulated trap profiles and intercepted DEP forces using average positioning deviations as X components; and (c) the schematic of two traps with different sizes.

objects in varied electric field.⁷ Shown in Figure 2(e) (solid lines) are the normalized simulation results of the trap profiles and the measured results (data points). The simulation results were found to be an order of magnitude stronger than the measured results showing that the real OET trap differs from this ideal simulated case. The difference between the simulated and the measured results is mainly due to the limitation of the ideal 2D simulation model. We are currently developing a 3D simulation model, which is closer to the reality. After normalizing the simulation results based on the measured peak DEP force, the shape of the simulation data matches up with the measured data very well and provides useful information of the trap profiles. To analyze the circular region where the stiction force dominates, the data of the average position deviation shown in Figure 3(i) were used as the radius of the circular region for each trap. For this circular region, the DEP force dominates outside it while the stiction force dominates inside it. Therefore, the stiction force should be equal to the DEP force at the boundary, which can be calculated using the average positioning deviation as the X component to intercept each simulated trap profile, as shown in Figure 4(b). It was found that the stiction forces of different traps are very similar to each other in the range of 0.070–0.105 nN. As the beads are free to roll across the surface of the device, they would experience a relatively low friction force based on a coefficient of rolling friction. This would give a much smaller stiction force than would be experienced by two parallel plates moving against each other.¹⁰ This points to this stiction force being mainly due to DEP forces pulling the beads towards the surface and electrostatic friction between the surfaces of the bead and a-Si:H layer. Since the solder beads feel similar stiction forces to keep them motionless regardless of the trap size and also the smaller trap has steeper trap profile in its central region, it requires a smaller trap with a smaller positioning displacement to generate enough DEP force to compensate the stiction force, whereas a larger trap needs a larger positioning displacement, thus showing a relatively poorer positioning accuracy. To provide visualized explanation, a schematic of two different-size traps is shown in Figure 4(c). The area inside the trap where the stiction force dominates (grey region) increases with the increase of trap size, indicating the reduced capability of a larger trap to position solder beads accurately compared with a smaller trap. This work

shows that although a large trap has a similar strong DEP force to a small trap at the edge of the trap and the solder bead feels a similar stiction force regardless of the trap size, the smaller trap shows better capability to position the bead accurately due to its steep central trap profile. For applications such as positioning and moving the bead over a long distance at high velocities with little requirement on positioning accuracy, both larger and smaller traps work similarly well. However, for applications such as fine positioning and highly accurate assembly of the beads, it is more desirable to use smaller traps. Our future plan in this area is to develop a method to remove the liquid medium in the OET device based on freeze-drying, which allows the assembled solder beads to be fixed in place after the liquid medium is removed.

In conclusion, we have demonstrated the use of OETs to manipulate 45 μm diameter solder beads with nN DEP force and sub-micron positioning accuracy. It was found that there is a dependence of positioning accuracy on the trap size, which is caused by stiction from electrically induced frictional forces. The experimental work is also supported by relevant simulations. This result is important for future work on the accurate assembly of electronic components and construction of circuits in OETs.

This work was supported by EPSRC (UK) under Grant Nos. EP/L022257/1 and EP/L00044X/1.

¹P. Y. Chiou, A. T. Ohta, and M. C. Wu, *Nature* **436**, 370 (2005).

²S. L. Neale, A. T. Ohta, H. Hsu, J. K. Valley, A. Jamshidi, and M. C. Wu, *Opt. Express* **17**, 5231 (2009).

³S.-M. Yang, T.-M. Yu, H.-P. Huang, M.-Y. Ku, L. Hsu, and C.-H. Liu, *Opt. Lett.* **35**, 1959 (2010).

⁴A. Jamshidi, P. J. Pauzauskie, P. J. Schuck, A. T. Ohta, P.-Y. Chiou, J. Chou, P. Yang, and M. C. Wu, *Nat. Photonics* **2**, 86 (2008).

⁵S. Zhang, J. M. Cooper, and S. L. Neale, *Proc. SPIE* **9759**, 97590S (2016).

⁶A. Jamshidi, S. L. Neale, K. Yu, P. J. Pauzauskie, P. J. Schuck, J. K. Valley, H.-Y. Hsu, A. T. Ohta, and M. C. Wu, *Nano Lett.* **9**, 2921 (2009).

⁷J. Juvert, S. Zhang, I. Eddie, C. J. Mitchell, G. T. Reed, J. S. Wilkinson, A. Kelly, and S. L. Neale, *Opt. Express* **24**, 18163 (2016).

⁸S. Zhang, J. Juvert, J. M. Cooper, and S. L. Neale, *Sci. Rep.* **6**, 32840 (2016).

⁹S. L. Neale, M. Mazilu, J. I. B. Wilson, K. Dholakia, and T. F. Krauss, *Opt. Express* **15**, 12619 (2007).

¹⁰N. Tasy, T. Sonnenberg, H. Jansen, R. Legtenberg, and M. Elwenspoek, *J. Micromech. Microeng.* **6**, 385–397 (1996).